Journal of Power Sources 195 (2010) 6043–6048

Contents lists available at ScienceDirect

Journal of Power Sources

journal homepage: www.elsevier.com/locate/jpowsour

Synthesis and electrochemical performances of core-shell structured $Li[(Ni_{1/3}Co_{1/3}Mn_{1/3})_{0.8}(Ni_{1/2}Mn_{1/2})_{0.2}]O_2$ cathode material for lithium ion batteries

Ki-Soo Lee [a], Seung-Taek Myung [b,*], Yang-Kook Sun [a,**]

[a] Department of Energy Engineering, Hanyang University, Seoul 133-791, South Korea
[b] Department of Chemical Engineering, Iwate University, 4-3-5 Ueda, Morioka, Iwate 020-8551, Japan

ARTICLE INFO

Article history:
Received 8 October 2009
Received in revised form 1 February 2010
Accepted 1 February 2010
Available online 6 February 2010

Keywords:
Co-precipitation
Core-shell
Cathode materials
Lithium ion batteries

ABSTRACT

Micro-scale core-shell structured $Li[(Ni_{1/3}Co_{1/3}Mn_{1/3})_{0.8}(Ni_{1/2}Mn_{1/2})_{0.2}]O_2$ powders for use as cathode material are synthesized by a co-precipitation method. To protect the core material $Li[Ni_{1/3}Co_{1/3}Mn_{1/3}]O_2$ from structural instability at high voltage, a $Li[Ni_{1/2}Mn_{1/2}]O_2$ shell, which provides structural and thermal stability, is used to encapsulate the core. A mixture of the prepared core-shell precursor and lithium hydroxide is calcined at 770 °C for 12 h in air. X-ray diffraction studies reveal that the prepared material has a typical layered structure with an $R\bar{3}m$ space group. Spherical morphologies with mono-dispersed powders are observed in the cross-sectional images obtained by scanning electron microscopy. The core-shell $Li[(Ni_{1/3}Co_{1/3}Mn_{1/3})_{0.8}(Ni_{1/2}Mn_{1/2})_{0.2}]O_2$ electrode has an excellent capacity retention at 30 °C, maintaining 99% of its initial discharge capacity after 100 cycles in the voltage range of 3–4.5 V. Furthermore, the thermal stability of the core-shell material in the highly delithiated state is improved compared to that of the core material. The resulting exothermic onset temperature appear at approximately 272 °C, which is higher than that of the highly delithiated $Li[Ni_{1/3}Co_{1/3}Mn_{1/3}]O_2$ (261 °C).

1. Introduction

Lithium ion batteries are considered potential energy storage devices for electric vehicles (EVs) and hybrid electric vehicles (HEVs). The most generally used commercial cathode material for lithium ion batteries is $LiCoO_2$ because of its excellent electrochemical performances [1]. However, it has limitations such as toxicity, high cost, and instability at high voltages (above 4.3 V) [2–4]. $Li[(Ni_{1/2}Mn_{1/2})_{1-x}Co_x]O_2$ (x = 0–0.333) has been used as an alternative positive electrode material for lithium ion batteries in an attempt to solve those problems [5–10]. Among the potential materials, $Li[Ni_{1/3}Co_{1/3}Mn_{1/3}]O_2$ has been studied as a promising cathode material for lithium ion batteries. It shows a high reversible capacity, good cycling performance, and thermal stability [11–13]. Furthermore, it delivers high reversible capacity by raising the upper cut-off voltage limit. However, the higher discharge capacity is accompanied by unstable cycling performance caused by structural disruption of the host structure.

In this study, a novel approach was attempted to achieve good cell performance. To further protect the $Li[Ni_{1/3}Co_{1/3}Mn_{1/3}]O_2$ core, the core was encapsulated by $Li[Ni_{1/2}Mn_{1/2}]O_2$. Through the formation of the core-shell architecture, a synergetic effect of the positive attributes of the two materials was expected. Namely, a higher capacity with moderate thermal stability from the $Li[Ni_{1/3}Co_{1/3}Mn_{1/3}]O_2$ core and superior cycling stability as well as an improved thermal property at high voltages from the $Li[Ni_{1/2}Mn_{1/2}]O_2$ shell were expected. In this study, we evaluated the structural, electrochemical, and thermal characteristics of the $Li[(Ni_{1/3}Co_{1/3}Mn_{1/3})_{0.8}(Ni_{1/2}Mn_{1/2})_{0.2}]O_2$ core-shell structure.

2. Experimental

$[Ni_{1/3}Co_{1/3}Mn_{1/3}](OH)_2$, $[(Ni_{1/3}Co_{1/3}Mn_{1/3})_{0.8}(Ni_{1/2}Mn_{1/2})_{0.2}](OH)_2$, and $[Ni_{1/2}Mn_{1/2}](OH)_2$ hydroxides were synthesized via co-precipitation. An aqueous solution of $NiSO_4$, $CoSO_4$, and $MnSO_4$ with a concentration of 2.0 mol dm^{-3} was pumped into a continuously stirred tank reactor under a nitrogen atmosphere. At the same time, a NaOH solution (*aq.*) of 2.0 mol dm^{-3} and a desired amount of NH_4OH solution (*aq.*) as a chelating agent were also separately fed into the reactor. During the co-precipitation reaction, initially formed particles grew into spherical particles under vigorous stirring. In order to construct the core-shell material with a composition of $[(Ni_{1/3}Co_{1/3}Mn_{1/3})_{0.8}(Ni_{1/2}Mn_{1/2})_{0.2}](OH)_2$, the obtained $[Ni_{1/3}Co_{1/3}Mn_{1/3}](OH)_2$ was continuously mixed with the solution containing metal compounds (cationic ratio of Ni:Mn = 1:1). Then, the obtained $[(Ni_{1/3}Co_{1/3}Mn_{1/3})_{0.8}(Ni_{1/2}Mn_{1/2})_{0.2}](OH)_2$ particles were filtered,

* Corresponding author. Tel.: +81 19 621 6345; fax: +81 19 621 6345.
** Corresponding author. Tel.: +82 2 2220 0524; fax: +82 2 2282 7329.
E-mail addresses: smyung@iwate-u.ac.jp (S.-T. Myung), yksun@hanyang.ac.kr (Y.-K. Sun).

0378-7753/$ – see front matter © 2010 Elsevier B.V. All rights reserved.
doi:10.1016/j.jpowsour.2010.02.002

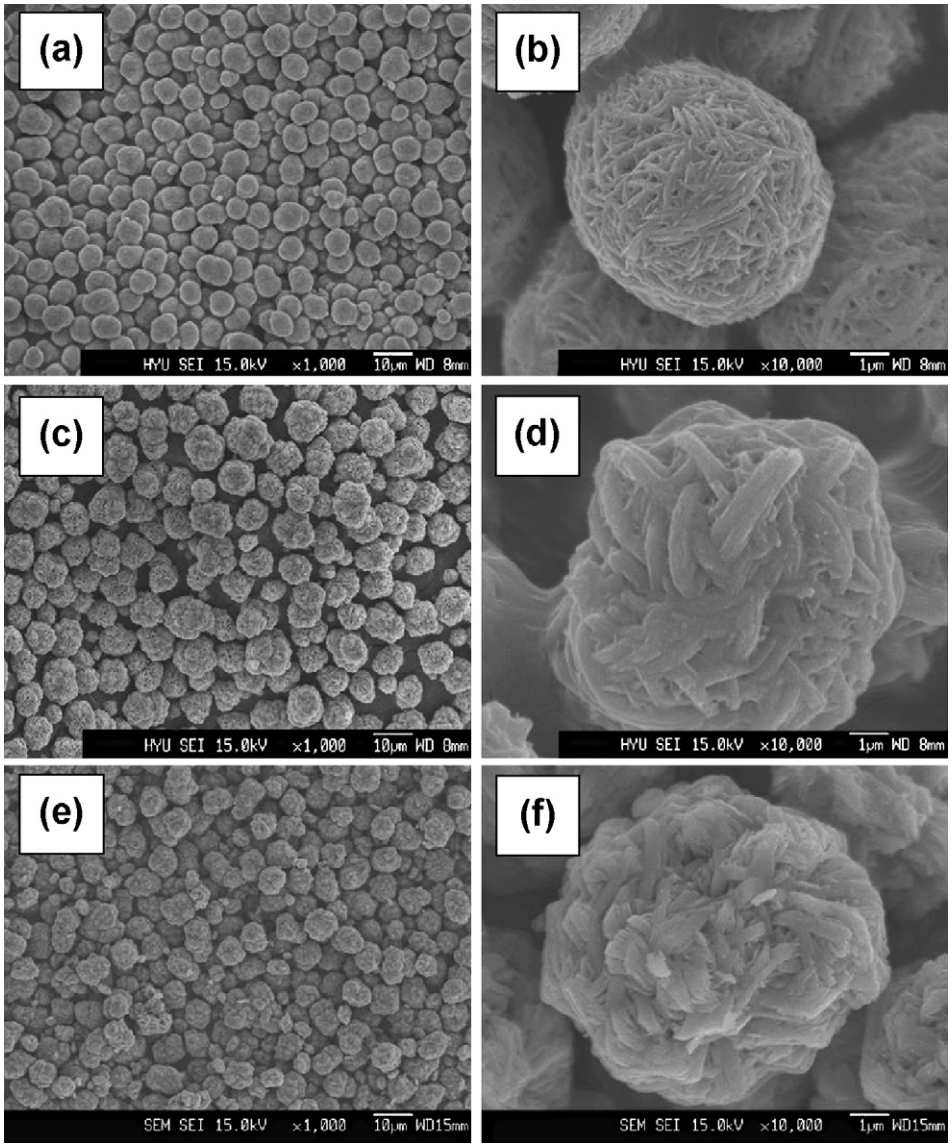

Fig. 1. SEM images of (a) low- and (b) high-magnification of $[Ni_{1/3}Co_{1/3}Mn_{1/3}](OH)_2$; (c) low- and (d) high-magnification of $[(Ni_{1/3}Co_{1/3}Mn_{1/3})_{0.8}(Ni_{1/2}Mn_{1/2})_{0.2}](OH)_2$; (e) low- and (f) high-magnification of $[Ni_{1/2}Mn_{1/2}](OH)_2$.

washed, and dried in air or under vacuum. The mixture of the obtained $[(Ni_{1/3}Co_{1/3}Mn_{1/3})_{0.8}(Ni_{1/2}Mn_{1/2})_{0.2}](OH)_2$ and $LiOH{\cdot}H_2O$ powders was preheated to 500 °C for 5 h and subsequently calcined at 770 °C for 12 h in a furnace under air to form lithiated layered core-shell powders.

The crystalline phase was analyzed by powder X-ray diffraction (XRD, Rigaku, Rint-2000) using Cu Kα radiation. The XRD data were obtained at $2\theta = 10$–80°, with a step size of 0.03°. The morphology of the prepared powders was determined by scanning electron microscopy (SEM, JSM-6340F, JEOL). The chemical compositions of the final powders were determined by atomic absorption spectroscopy (AAS, Vario 6, AnalyticJena).

Electrochemical testing was performed in R2032 coin-type cells. The cathodes were fabricated by blending the prepared powders, Super P carbon black, and polyvinylidene fluoride (85:7.5:7.5) in *N*-methyl-2-pyrrolidone. The slurry was then applied to aluminum foil and dried at 110 °C for ten h in a vacuum oven. Finally, disks were punched out of the foil. The negative electrode was lithium foil, and the electrolyte was a 1 M $LiPF_6$ solution in an ethylene carbonate (EC)–diethyl carbonate (DEC) mixture (3:7 ratio by volume, UKSEUNG CHEMICAL Co. Ltd.). The cathode and anode were separated by a porous polypropylene film. All cells were prepared in an Ar-filled dry box. The assembled cells were charged and discharged in the voltage range of 3.0–4.5 V at a constant current density of 100 mA g^{-1} at 30 °C. Cycle-life tests were performed under the same voltage and temperature conditions.

Differential scanning calorimetry (DSC) experiments were carried out for the positive electrode material by fully charging the cells to 4.5 V. After the remaining electrolyte was carefully removed from the surface of the electrode, the positive electrode materials were recovered from the current collector (Al foil). A stainless steel sealed pan with a gold-plated copper seal, which had a capacity of 30 μL and was able to withstand a pressure of 150 atm before rupturing, was used to collect 3–5 mg samples. Measurements were carried out using a differential scanning calorimeter (NETZSCH-TA4, Germany) at a temperature scan rate of 5 °C min^{-1} in the temperature range of 100–350 °C.

3. Results and discussion

Fig. 1 shows the SEM images of the precursor powders prepared by co-precipitation. The particle shape was spherical, and

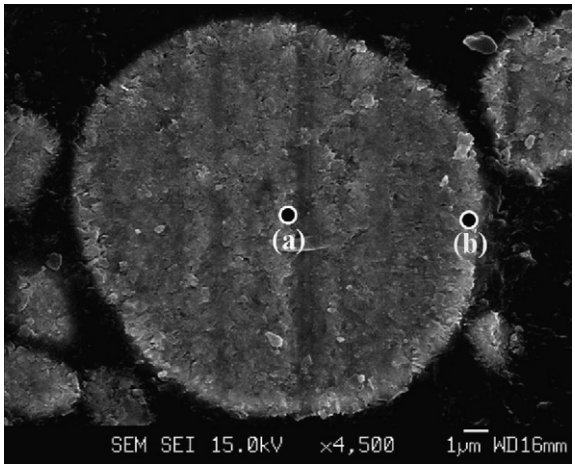

Fig. 2. Cross-section SEM image of precursor core-shell $[(Ni_{1/3}Co_{1/3}Mn_{1/3})_{0.8}(Ni_{1/2}Mn_{1/2})_{0.2}](OH)_2$ particle.

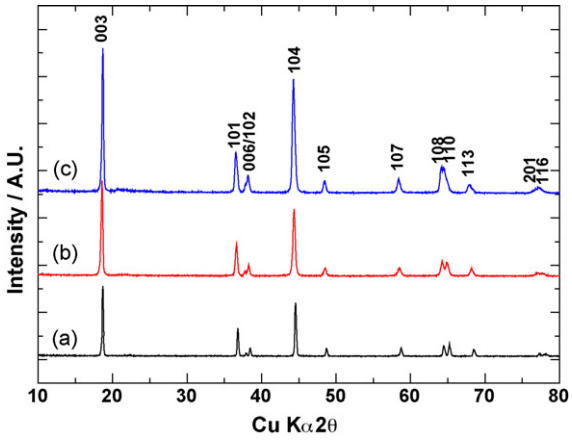

Fig. 3. X-ray diffraction patterns of (a) core $Li[Ni_{1/3}Co_{1/3}Mn_{1/3}]O_2$, (b) core-shell $Li[(Ni_{1/3}Co_{1/3}Mn_{1/3})_{0.8}(Ni_{1/2}Mn_{1/2})_{0.2}]O_2$ and (c) shell $Li[Ni_{0.5}Mn_{0.5}]O_2$.

the estimated average particle diameter of the core-shell structured $[(Ni_{1/3}Co_{1/3}Mn_{1/3})_{0.8}(Ni_{1/2}Mn_{1/2})_{0.2}](OH)_2$ in Fig. 1b and c was about 10 μm, which was slightly larger than that of the core material (8 μm) in Fig. 1a and b, implying that the core was encapsulated by the $[Ni_{1/2}Mn_{1/2}](OH)_2$ shell. $[Ni_{1/2}Mn_{1/2}](OH)_2$ as a shell material was also synthesized via co-precipitation for comparison. From the SEM images in Fig. 1d and f, it was confirmed that the sediment particle shapes for the core-shell hydroxide (Fig. 1d) were similar to that of the shell (Fig. 1f). In the case of the core, the primary particles had a needle-like shape and agglomerated in secondary forms, as seen in Fig. 1b. The chemical composition of the synthesized core-shell structured powders was $[Ni_{0.375}Co_{0.241}Mn_{0.384}](OH)_2$, as determined by atomic absorption spectroscopy. The composition can therefore be written in the core-shell notation as $[(Ni_{1/3}Co_{1/3}Mn_{1/3})_{0.8}(Ni_{1/2}Mn_{1/2})_{0.2}](OH)_2$.

The cross-sectional SEM image of the precursor $[(Ni_{1/3}Co_{1/3}Mn_{1/3})_{0.8}(Ni_{1/2}Mn_{1/2})_{0.2}](OH)_2$ particle showed that the particle was divided into two parts, based on the contrast seen in Fig. 2, with the core in the center and the shell on the outside. The thickness of the shell was approximately 1 μm, as measured from the outer surface to the particle interior. From the EPMA data, the deduced chemical composition of point (a) was found to be $[Ni_{0.336}Co_{0.326}Mn_{0.338}](OH)_2$, which is close to the ideal core composition of $[Ni_{1/3}Co_{1/3}Mn_{1/3}](OH)_2$. The chemical composition of point (c) in the shell was $[Ni_{0.492}Co_{0.008}Mn_{0.500}](OH)_2$. As designed, these compositions indicate that the core-shell structured precursor was synthesized by co-precipitation.

The as-prepared core-shell $[(Ni_{1/3}Co_{1/3}Mn_{1/3})_{0.8}(Ni_{1/2}Mn_{1/2})_{0.2}](OH)_2$ was thoroughly mixed with lithium hydroxide and the mixture was calcined at 770 °C for 12 h in an ambient atmosphere. When the calcination temperature was reduced, the resulting crystallinity of the final product was lowered. Alternatively, high temperature calcination gave rise to severe diffusion of cations into the core-shell structure. Therefore, there was an optimum temperature that gave good crystallinity and lower cation mixing within the core-shell particle. Fig. 3 shows X-ray diffraction patterns of the as-calcined core, core-shell, and shell powders. All of the powders were confirmed to have a well-defined hexagonal α-$NaFeO_2$-type structure with a space group of $R\bar{3}m$. No impurities were observed in the XRD patterns. However, subtle changes in the (1 0 8) and (1 1 0) peaks were found in the XRD patterns. In fact, a sharp splitting in the (1 0 8) and (1 1 0) peaks can be seen in Fig. 3a. Although the splitting for the core-shell structured $Li[(Ni_{1/3}Co_{1/3}Mn_{1/3})_{0.8}(Ni_{1/2}Mn_{1/2})_{0.2}]O_2$ was clear, it was not as clear for the $Li[Ni_{1/3}Co_{1/3}Mn_{1/3}]O_2$ in Fig. 3a. In the case of the shell material, the (1 0 8) and (1 1 0) peaks merged together, as shown in Fig. 3c. Overlaying of the XRD patterns of the core $Li[Ni_{1/3}Co_{1/3}Mn_{1/3}]O_2$ and the shell $Li[Ni_{0.5}Mn_{0.5}]O_2$ results in reduced peak splitting of the (1 0 8) and (1 1 0) peaks.

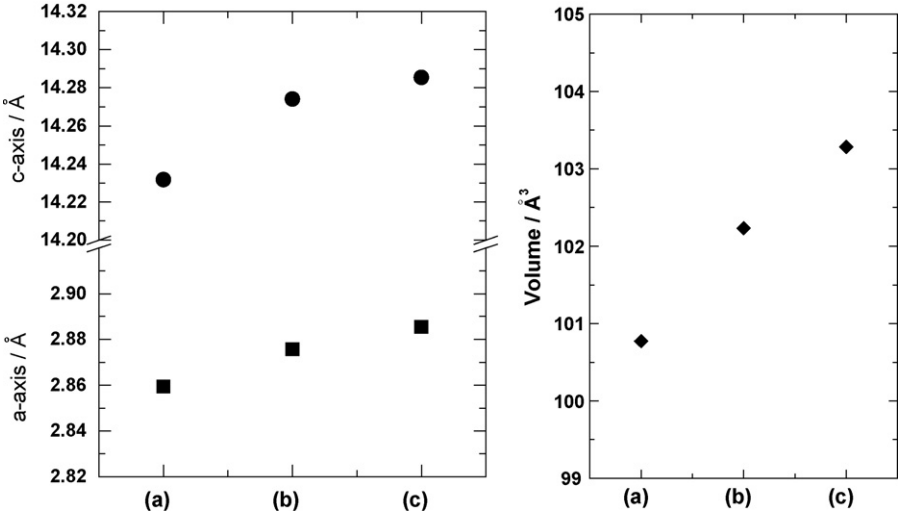

Fig. 4. Variation in lattice parameter of (a) core $Li[Ni_{1/3}Co_{1/3}Mn_{1/3}]O_2$, (b) core-shell $Li[(Ni_{1/3}Co_{1/3}Mn_{1/3})_{0.8}(Ni_{1/2}Mn_{1/2})_{0.2}]O_2$ and (c) shell $Li[Ni_{0.5}Mn_{0.5}]O_2$.

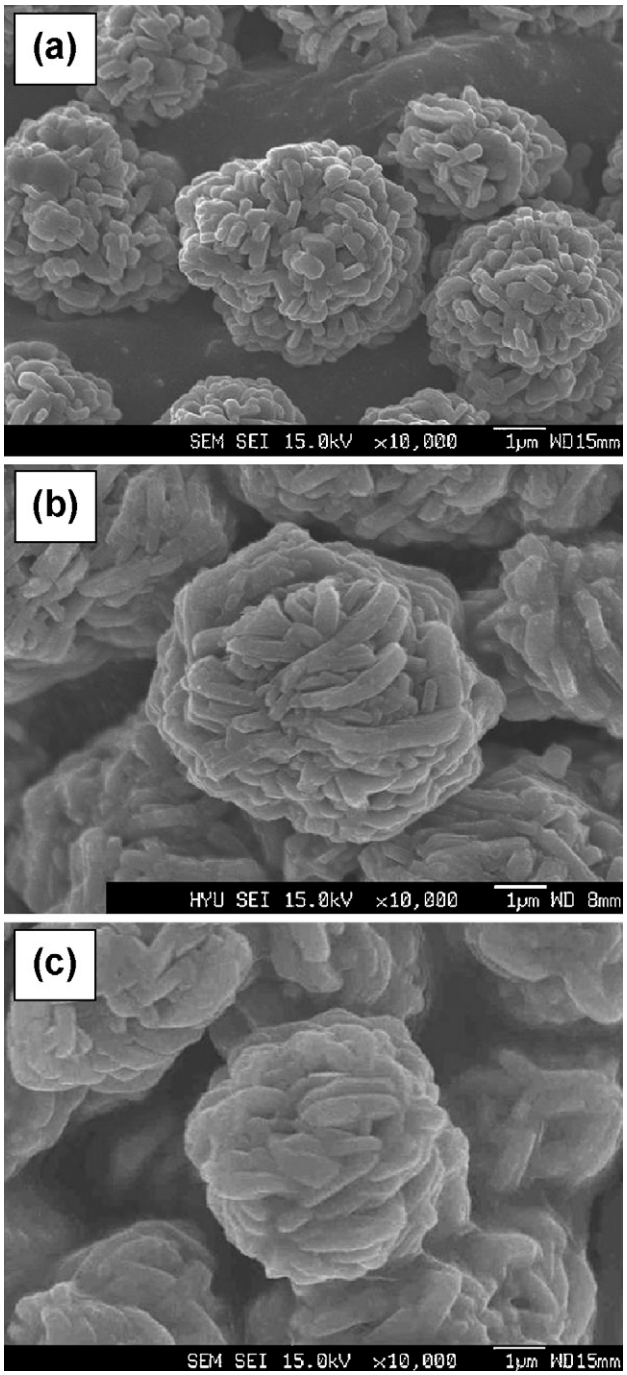

Fig. 5. SEM image of (a) core $Li[Ni_{1/3}Co_{1/3}Mn_{1/3}]O_2$, (b) core-shell $Li[(Ni_{1/3}Co_{1/3}Mn_{1/3})_{0.8}(Ni_{1/2}Mn_{1/2})_{0.2}]O_2$ and (c) shell $Li[Ni_{0.5}Mn_{0.5}]O_2$ particle.

From the XRD patterns in Fig. 3, we calculated the lattice parameters by a least squares method assuming the structural model of $R\bar{3}m$. Fig. 4 shows the lattice parameters of the core, core-shell, and shell powders. The lattice parameters for the core-shell powders were somewhat greater than those of $Li[Ni_{1/3}Co_{1/3}Mn_{1/3}]O_2$, but they were smaller than those of $Li[Ni_{0.5}Mn_{0.5}]O_2$. The overlaying of the XRD patterns of $Li[Ni_{1/3}Co_{1/3}Mn_{1/3}]O_2$ and $Li[Ni_{0.5}Mn_{0.5}]O_2$ and the presence of $Li[Ni_{0.5}Mn_{0.5}]O_2$ on the $Li[Ni_{1/3}Co_{1/3}Mn_{1/3}]O_2$ core probably led to the variation in the lattice parameters. Provided that each compound exists in the powders, the resulting $Li[Ni_{1/3}Co_{1/3}Mn_{1/3}]O_2$ and $Li[Ni_{0.5}Mn_{0.5}]O_2$ should individually appear in the XRD patterns. The elemental ratio of the transition metals was close to that of the core-shell hydroxide, indicating that no evaporation of transition metals occurred during the calcination stage.

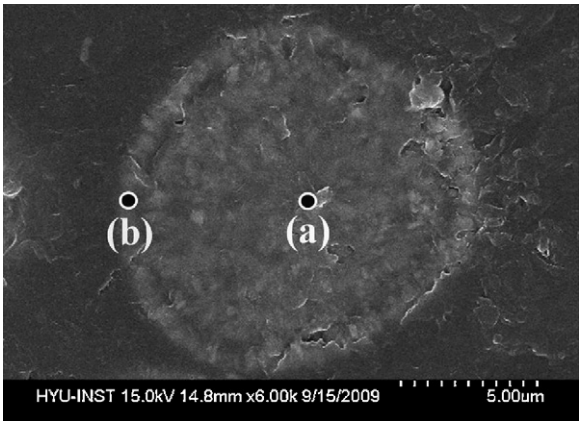

Fig. 6. Cross-section SEM image of core-shell $Li[(Ni_{1/3}Co_{1/3}Mn_{1/3})_{0.8}(Ni_{1/2}Mn_{1/2})_{0.2}]O_2$ particle.

SEM images of the lithiated powders at high temperature are shown in Fig. 5. It was obvious that the needle-shaped primary particles of $[Ni_{1/3}Co_{1/3}Mn_{1/3}](OH)_2$ seen in Fig. 1a changed to the rectangular-shaped primary particles observed in Fig. 5a. Also, there was no disruption of the particle morphology for the core-shell $Li[(Ni_{1/3}Co_{1/3}Mn_{1/3})_{0.8}(Ni_{1/2}Mn_{1/2})_{0.2}]O_2$ in Fig. 5b, since the two different hydroxide compositions would cause a different shrinkage ratio during the high temperature calcination process. Changes in the primary particle morphologies for the core-shell and $Li[Ni_{0.5}Mn_{0.5}]O_2$ were not very obvious in Fig. 5b and c, compared to the hydroxides in Fig. 1d and f. The similarity of the particle morphologies implies that the outer $Li[Ni_{0.5}Mn_{0.5}]O_2$ shell completely surrounded the inner $Li[Ni_{1/3}Co_{1/3}Mn_{1/3}]O_2$ core.

Therefore, a cross-sectional SEM image of the core-shell $Li[(Ni_{1/3}Co_{1/3}Mn_{1/3})_{0.8}(Ni_{1/2}Mn_{1/2})_{0.2}]O_2$ particles was taken and is shown in Fig. 6. As seen in Fig. 5b, the inner core was completely encapsulated by the outer shell with a thickness of about 1 μm. Structural mismatch causing hollow holes was not observed in the SEM image. For the hydroxide, the chemical compositions of the core-shell hydroxides were $[Ni_{0.336}Co_{0.326}Mn_{0.338}](OH)_2$ for the core and $[Ni_{0.492}Co_{0.008}Mn_{0.500}](OH)_2$ for the shell. Similarly, EPMA was employed to deduce the chemical composition of the lithiated core-shell $Li[(Ni_{1/3}Co_{1/3}Mn_{1/3})_{0.8}(Ni_{1/2}Mn_{1/2})_{0.2}]O_2$. The core had a chemical composition of $Li[Ni_{0.339}Co_{0.329}Mn_{0.332}]O_2$, indicating that Co diffused into the Co-deficient shell. The chemical composition of the shell was found to be $Li[Ni_{0.474}Co_{0.054}Mn_{0.472}]O_2$. There was no Co in the $Li[Ni_{0.5}Mn_{0.5}]O_2$ shell so a concentration gradient of Co was likely to occur, resulting in incorporation of Co in the shell.

Fig. 7a and b shows the first charge–discharge curves and the differentiated curves, respectively, obtained from $Li[Ni_{1/3}Co_{1/3}Mn_{1/3}]O_2$ core, core-shell $Li[(Ni_{1/3}Co_{1/3}Mn_{1/3})_{0.8}(Ni_{1/2}Mn_{1/2})_{0.2}]O_2$, and $Li[Ni_{0.5}Mn_{0.5}]O_2$ shell. The electrochemical performance was measured at 30 °C with a constant current density of 100 mA g^{-1} applied over a voltage range of 3.0–4.5 V versus Li. The initial charge–discharge capacities of the core and core-shell electrodes were similar at 180.5 mAh g^{-1} (core), 177.0 mAh g^{-1} (core-shell), and 156.2 mAh g^{-1} (shell). In spite of the lower specific discharge capacity of the shell material, the core-shell material delivered high capacity in the voltage range of 3.0–4.5 V. The discharge curves shown in Fig. 7a were differentiated to produce the results in Fig. 7b. The resulting discharge voltage of the core-shell material was slightly lower than that of the core $Li[Ni_{1/3}Co_{1/3}Mn_{1/3}]O_2$. However, the shape of the differentiated curve in Fig. 7b–d for

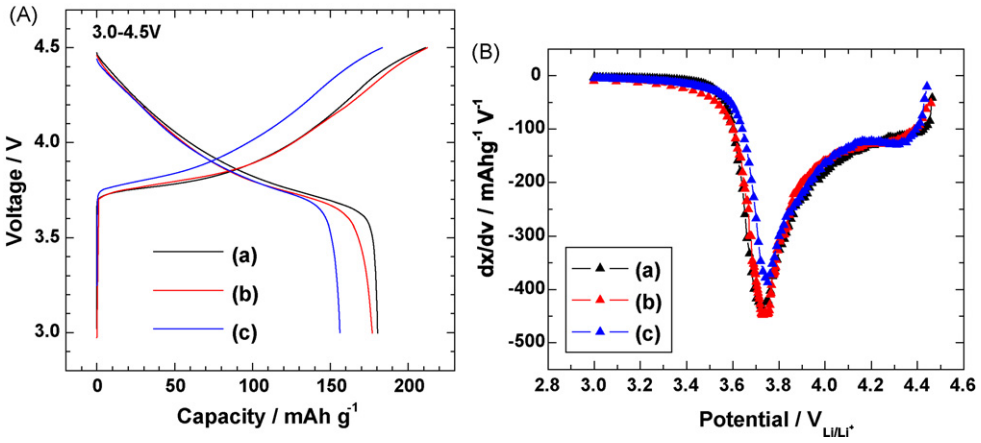

Fig. 7. (A) Comparison of the first charge and discharge curves of (a) core $Li[Ni_{1/3}Co_{1/3}Mn_{1/3}]O_2$, (b) core-shell $Li[(Ni_{1/3}Co_{1/3}Mn_{1/3})_{0.8}(Ni_{1/2}Mn_{1/2})_{0.2}]O_2$ and (c) shell $Li[Ni_{0.5}Mn_{0.5}]O_2$ cells. (B) Corresponding differentiated curves for discharge of (a)–(c).

the discharge was not similar to that of the $Li[Ni_{0.5}Mn_{0.5}]O_2$ shell (Fig. 7b and c) at higher voltages.

Fig. 8 shows the continuous charge–discharge curves and cyclabilities of the $Li[Ni_{1/3}Co_{1/3}Mn_{1/3}]O_2$ core, $Li[(Ni_{1/3}Co_{1/3}Mn_{1/3})_{0.8}(Ni_{1/2}Mn_{1/2})_{0.2}]O_2$ core-shell, and $Li[Ni_{0.5}Mn_{0.5}]O_2$ shell electrodes over 100 cycles. The core $Li[Ni_{1/3}Co_{1/3}Mn_{1/3}]O_2$ cell exhibited gradual capacity fading upon cycling (Fig. 8a), and the capacity retention was about 77.8% over 100 cycles (Fig. 8a–d). On the other hand, the core-shell structured $Li[(Ni_{1/3}Co_{1/3}Mn_{1/3})_{0.8}(Ni_{1/2}Mn_{1/2})_{0.2}]O_2$ cell showed good capacity retention (Fig. 8b), maintaining 98.8% of its initial capacity during the 100 cycles (Fig. 8b–d). Also, the $Li[Ni_{0.5}Mn_{0.5}]O_2$ electrodes had a similar cycling performance. The core-shell structure gave rise to a significant improvement in the high-voltage cycling performance, which was probably due to the impact of the $Li[Ni_{0.5}Mn_{0.5}]O_2$ shell. It is most likely that the $Li[Ni_{0.5}Mn_{0.5}]O_2$ shell protected the structural deformation of the core $Li[Ni_{1/3}Co_{1/3}Mn_{1/3}]O_2$ material at high voltage. Thus, rapid capacity fading of the core material was buffered by the encapsulation by $Li[Ni_{0.5}Mn_{0.5}]O_2$. From this result, it is believed that the structural instability of the core was successfully overcome by the construction of the core-shell architecture.

Fig. 9 shows the DSC profiles of the core, core-shell, and shell electrodes charged to 4.5 V. Each material showed dif-

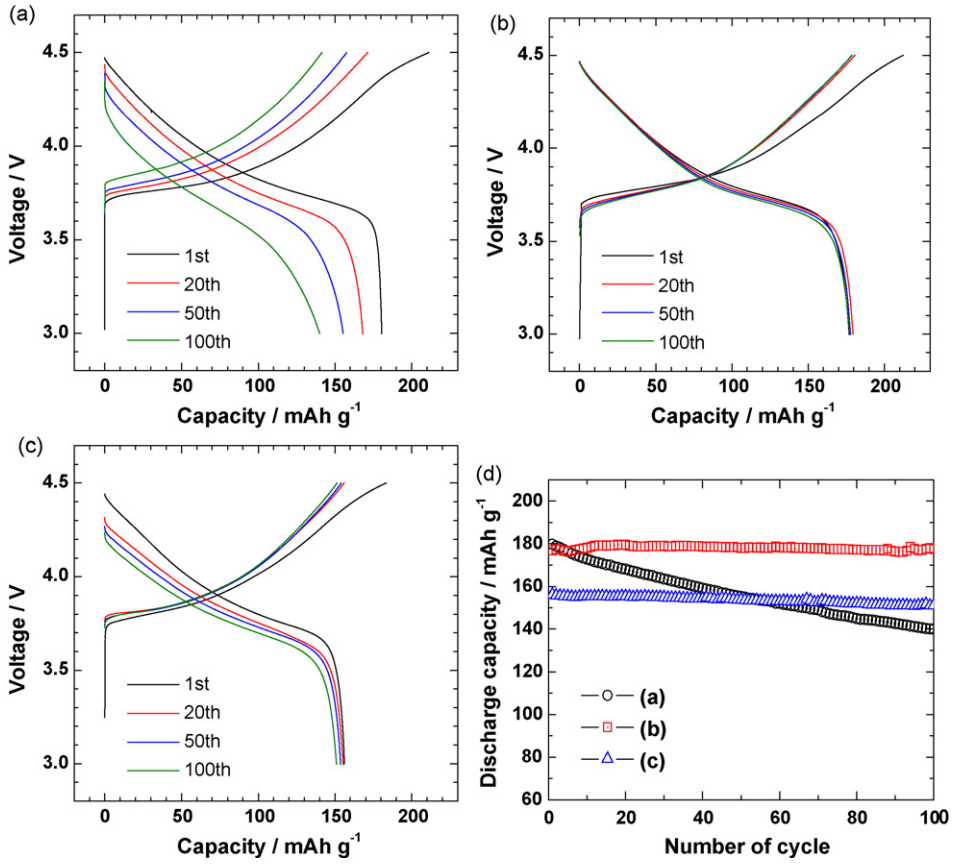

Fig. 8. Continuous charge and discharge curves of (a) core $Li[Ni_{1/3}Co_{1/3}Mn_{1/3}]O_2$, (b) core-shell $Li[(Ni_{1/3}Co_{1/3}Mn_{1/3})_{0.8}(Ni_{1/2}Mn_{1/2})_{0.2}]O_2$ and (c) shell $Li[Ni_{0.5}Mn_{0.5}]O_2$ cells; (d) cyclability of Li/(a), (b) and (c) cells at 30 °C.

Table 1
Comparison of lattice parameters of the extensively cycled electrodes for the core $Li[Ni_{1/3}Co_{1/3}Mn_{1/3}]O_2$ and core-shell $Li[(Ni_{1/3}Co_{1/3}Mn_{1/3})_{0.8}(Ni_{1/2}Mn_{1/2})_{0.2}]O_2$.

	Crystal parameters		
	a/Å	c/Å	Vol/Å^3
Core $Li[Ni_{1/3}Co_{1/3}Mn_{1/3}]O_2$	2.8577 (2)	14.2286 (1)	99.85
Core-shell $Li[(Ni_{1/3}Co_{1/3}Mn_{1/3})_{0.8}(Ni_{1/2}Mn_{1/2})_{0.2}]O_2$	2.8755 (1)	14.2738 (1)	102.14

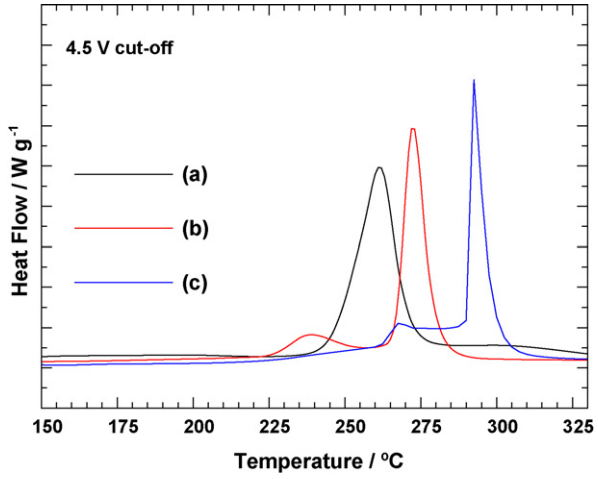

Fig. 9. DSC profiles of (a) core $Li[Ni_{1/3}Co_{1/3}Mn_{1/3}]O_2$, (b) core-shell $Li[(Ni_{1/3}Co_{1/3}Mn_{1/3})_{0.8}(Ni_{1/2}Mn_{1/2})_{0.2}]O_2$ and (c) shell $Li[Ni_{0.5}Mn_{0.5}]O_2$.

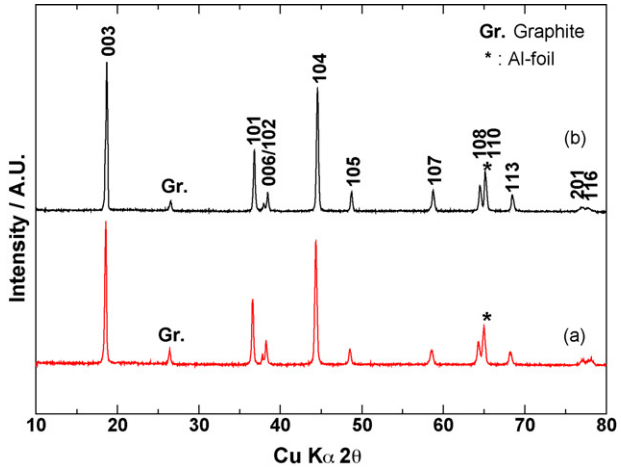

Fig. 10. X-ray diffraction patterns of (a) core $Li[Ni_{1/3}Co_{1/3}Mn_{1/3}]O_2$ and (b) core-shell $Li[(Ni_{1/3}Co_{1/3}Mn_{1/3})_{0.8}(Ni_{1/2}Mn_{1/2})_{0.2}]O_2$ electrodes after 100cycles.

ferent tendencies for heat generation. A large exothermic peak of the core $Li[Ni_{1/3}Co_{1/3}Mn_{1/3}]O_2$ material appeared at 261.5 °C. A sharp exothermic peak for the delithiated $Li[(Ni_{1/3}Co_{1/3}Mn_{1/3})_{0.8}(Ni_{1/2}Mn_{1/2})_{0.2}]O_2$ was found at 272 °C, accompanying by a small exothermic peak at 240 °C. For the core-shell powders, the outer shell was composed of $Li[Ni_{0.5}Mn_{0.5}]O_2$. Although the exothermic temperature of $Li[Ni_{0.5}Mn_{0.5}]O_2$ shifted to a higher temperature (292 °C for the main reaction), the profile coincided well with that of the core-shell $Li[(Ni_{1/3}Co_{1/3}Mn_{1/3})_{0.8}(Ni_{1/2}Mn_{1/2})_{0.2}]O_2$. The reason for the improved thermal properties of $Li[Ni_{0.5}Mn_{0.5}]O_2$ was that the absence of tetravalent Co and the presence of tetravalent Mn in the shell improved the thermal stability. Furthermore, the Ni valence did not completely reach the tetravalent state even in the highly delithiated state. In consideration of the above effect, the observed improvement in the thermal properties of the core-shell powders, as compared with the core material, is understandable.

Fig. 10 shows the XRD patterns of the cycled core $Li[Ni_{1/3}Co_{1/3}Mn_{1/3}]O_2$ and core-shell $Li[(Ni_{1/3}Co_{1/3}Mn_{1/3})_{0.8}(Ni_{1/2}Mn_{1/2})_{0.2}]O_2$ electrodes. The single-phase layered structure with an $R\bar{3}m$ was maintained throughout cycling for both electrodes and impurities were not observed in the XRD patterns. The lattice parameters were calculated from the XRD patterns using a least squares method. The lattice parameters for the core-shell $Li[(Ni_{1/3}Co_{1/3}Mn_{1/3})_{0.8}(Ni_{1/2}Mn_{1/2})_{0.2}]O_2$ electrode were almost identical to those of the original material prior to cycling, while the lattice parameters decreased slightly for the core $Li[Ni_{1/3}Co_{1/3}Mn_{1/3}]O_2$ in Table 1. Based on this data, less structural change occurred for the core-shell $Li[(Ni_{1/3}Co_{1/3}Mn_{1/3})_{0.8}(Ni_{1/2}Mn_{1/2})_{0.2}]O_2$ electrode.

4. Conclusions

Spherical $[(Ni_{1/3}Co_{1/3}Mn_{1/3})_{0.8}(Ni_{1/2}Mn_{1/2})_{0.2}](OH)_2$ compounds were obtained through co-precipitation. The thickness of the shell $Li[Ni_{1/2}Mn_{1/2}]O_2$ in the core-shell material was approximately 1 μm. XRD revealed that the prepared core-shell material had a single-phase layered structure with an $R\bar{3}m$ space group. A high capacity was obtained from the $Li[Ni_{1/3}Co_{1/3}Mn_{1/3}]O_2$ core, while structural stability was derived from the $Li[Ni_{1/2}Mn_{1/2}]O_2$ shell. The core-shell $Li[(Ni_{1/3}Co_{1/3}Mn_{1/3})_{0.8}(Ni_{1/2}Mn_{1/2})_{0.2}]O_2$ electrode exhibited greatly enhanced cycling stability compared to that of the core $Li[Ni_{1/3}Co_{1/3}Mn_{1/3}]O_2$ at the high cut-off voltage of 4.5 V. The capacity retention of the core-shell electrode was about 98.8% of its initial capacity over 100 cycles. Based on the DSC results, the core-shell $Li[(Ni_{1/3}Co_{1/3}Mn_{1/3})_{0.8}(Ni_{1/2}Mn_{1/2})_{0.2}]O_2$ electrode charged to 4.5 V showed improved thermal stability because of the thermal stability of the $Li[Ni_{1/2}Mn_{1/2}]O_2$ shell material.

Acknowledgement

This work was supported by the National Research Foundation of Korea (NRF) grant funded by the Korea government (MEST) (No. 2009-0092780).

References

[1] J.N. Reimers, J.R. Dahn, J. Electrochem. Soc. 139 (1992) 209.
[2] Z. Lu, D.D. MacNeil, J.R. Dahn, Electrochem. Solid-State Lett. 4 (2001) A200.
[3] D. MacNeil, Z. Lu, J.R. Dahn, J. Electrochem. Soc. 149 (2002) A1332.
[4] Y.-K. Sun, S.-T. Myung, H.J. Bang, B.-C. Park, S.-J. Park, N.-Y. Sung, J. Electrochem. Soc. 154 (2007) A937.
[5] T. Ohzuku, Y. Makimura, Chem. Lett. 30 (2001) 642.
[6] S.-T. Myung, Y.-K. Sun, Electrochim. Acta 50 (2005) 4800.
[7] T. Ohzuku, Y. Makimura, Chem. Lett. 30 (2001) 744.
[8] S.-M. Park, T.-H. Cho, M. Yoshio, Chem. Lett. 33 (2004) 6.
[9] M.-H. Lee, Y.-J. Kang, S.-T. Myung, Y.-K. Sun, Electrochim. Acta 50 (2004) 939.
[10] S.W. Oh, S.H. Park, C.-W. Park, Y.-K. Sun, Solid State Ionics 171 (2004) 167.
[11] G.-H. Kim, J.-H. Kim, S.-T. Myung, C.S. Yoon, Y.-K. Sun, J. Electrochem. Soc. 152 (2005) A1707.
[12] W. Lu, I. Belharouak, D. Vissers, K. Amine, J. Electrochem. Soc. 153 (2006) A2147.
[13] S.-T. Myung, S. Komaba, K. Hosoya, Y. Miura, N. Hirosaki, N. Kumagai, Chem. Mater. 17 (2005) 2427.